

Key Points:

- We characterized visible/near-infrared reflectance and midinfrared emissivity spectra of chloride salt-bearing assemblages
- We constrained detection limits of minor phase that could be present in chloride-bearing assemblages
- We suggested that additional minor phases could only be present at very low abundances in Martian chloride salt-bearing deposits

Supporting Information:

- Supporting Information S1

Correspondence to:

C. Ye,
cheng.ye.1@stonybrook.edu

Citation:

Ye, C., & Glotch, T. D. (2019). Spectral properties of chloride salt-bearing assemblages: Implications for detection limits of minor phases in chloride-bearing deposits on Mars. *Journal of Geophysical Research: Planets*, 124, 209–222. <https://doi.org/10.1029/2018JE005859>

Received 23 OCT 2018

Accepted 31 DEC 2018

Accepted article online 10 JAN 2019

Published online 1 FEB 2019

©2019. The Authors.

This is an open access article under the terms of the Creative Commons Attribution-NonCommercial-NoDerivs License, which permits use and distribution in any medium, provided the original work is properly cited, the use is non-commercial and no modifications or adaptations are made.

Spectral Properties of Chloride Salt-Bearing Assemblages: Implications for Detection Limits of Minor Phases in Chloride-Bearing Deposits on Mars

Cheng Ye¹  and Timothy D. Glotch¹ 

¹Department of Geosciences, Stony Brook University, Stony Brook, NY, USA

Abstract Chloride salt-bearing deposits have been identified throughout the southern highlands of Mars and have been suggested to be two component mixtures of anhydrous chloride salt and regional basaltic regolith. On Earth, chlorides typically occur as evaporite salts associated with other evaporite minerals such as carbonate and sulfate, and chemical weathering products like clays. In this laboratory study, we document the visible/near-infrared reflectance and midinfrared emissivity spectral characteristics of a series of chloride salt-bearing mineral assemblages. Our data show that the spectral features of various powder mixtures change systematically with variable additional mineral concentrations and particle sizes. Specifically, small amounts of calcite, gypsum, or nontronite have a relatively large effect on the bulk spectral properties of halite/labradorite mixtures making them easily distinguishable from two-component halite/labradorite mixtures. This fundamental laboratory work suggests that additional minor phases could only be present at no more than 1–5 wt% in Martian chloride salt-bearing deposits.

Plain Language Summary Chloride salt-bearing deposits have been identified throughout the southern highlands of Mars. Since these deposits could form through the evaporation of brines, they can indicate that water once was widespread and could remain over a long time in Martian ancient history. Chloride salt deposits are intriguing since they may be good at preserving past Martian life. Unlike evaporite salt deposits on Earth, which are usually a set of evaporite minerals, chloride salt-bearing deposits on Mars are isolated chloride salt mixed with regional basaltic soil. In this work, we use visible/near-infrared and midinfrared spectroscopy to characterize spectral features of a series of chloride salt-bearing mineral assemblages. We suggest that additional minor phases could only be present at very low abundances in Martian chloride salt-bearing deposits.

1. Introduction

Chloride salt-bearing deposits in the southern highlands of Mars have been observed and characterized by the Mars Odyssey Thermal Emission Imaging System (THEMIS), Mars Global Surveyor Thermal Emission Spectrometer (TES), Mars Reconnaissance Orbiter Compact Reconnaissance Imaging Spectrometer for Mars (CRISM), and Mars Express Observatoire pour la Minéralogie, l'Eau, les Glaces et l'Activité (OMEGA; Glotch et al., 2010, 2016; Murchie et al., 2009; Osterloo et al., 2008, 2010; Ruesch et al., 2012; Wray et al., 2009). The chloride salt-bearing deposits exhibit a distinctive blue slope (decrease in emissivity with increasing wavelength) over the 8–12 μm (midinfrared [MIR]) spectral range and a featureless red slope (increase in reflectance with increasing wavelength) relative to the surrounding terrain over the ~1–2.6 μm (visible/near-infrared [VNIR]) spectral range.

The unusual spectral properties of chloride salt-bearing deposits have been approximated by laboratory measurements of salt/silicate mixtures and light scattering models. Laboratory VNIR spectral measurements of mixtures of anhydrous chloride salt and silicates generally reproduce the characteristic spectra seen in CRISM data (Jensen & Glotch, 2011). Laboratory MIR emissivity spectra of halite/basalt mixtures and a hybrid T-matrix/Hapke light scattering model provide constraints on the abundances (10–25 wt%) and particle sizes (generally 63–180 μm , with a few instances of finely particulate <10- μm surfaces) of salt in the Martian chloride deposits (Glotch et al., 2016).

The discrete chloride-bearing deposits are generally located in topographically low terrains (Osterloo et al., 2008, 2010). A positive 3- μm feature in CRISM and OMEGA ratio spectra indicates that these deposits are desiccated compared to the surrounding terrain (Glotch et al., 2010, 2017; Murchie et al., 2009; Ruesch

et al., 2012). Glotch et al. (2010) conducted a spectroscopic and geological analysis of chloride salt deposits in Terra Sirenum, where chloride salt deposits are in close proximity to phyllosilicates, and suggested the formation of chlorides as a result of groundwater upwelling and evaporation. Hynek et al. (2015) suggested a late-stage chloride formation mechanism, likely as the result of the fluviolacustrine environment caused by surface water near Meridiani Planum. Polygonal cracking patterns in chloride-bearing terrains have been observed in High Resolution Imaging Science Experiment (HiRISE) images (Osterloo et al., 2008, 2010). El-Maarry et al. (2013, 2014) suggested that the presence of smectite-rich phyllosilicates is the main reason for development of these cracking patterns, prompting them to propose a close association of chlorides and phyllosilicates in these deposits, similar to their association in terrestrial salt-rich playa settings (Eugster & Hardie, 1978). These works, though providing different detailed suggestions for the depositional environments of these deposits, all present evidence that supports the interpretation of evaporative environments as a formation mechanism for chloride deposits on Mars.

However, chloride salt rarely occurs in isolation in evaporative environments. On Earth, evaporative systems typically display a variety of mineral assemblages on various spatial scales, including chlorides, carbonates, and sulfates (e.g., Eugster & Hardie, 1978). Tosca and McLennan (2006) evaluated chemical divides and brine evolution for Martian systems, which are largely controlled by basaltic crust weathering rather than granitic rocks as they are on Earth, and defined five brine evolution pathways. Of these pathways, three result in late-stage brines favoring chloride salt precipitation. In each case, the pathway to formation of these late-stage brines and precipitates includes the precipitation of carbonates and sulfates. However, chloride-bearing deposits on Mars appear to be two-component mixtures of chloride salt and the regional silicate regolith, and no additional evaporite minerals have been identified in relation to the chloride salt-bearing deposits. Also phyllosilicates, as the primary chemical weathering products, in some areas are in close association with chlorides but, as far as we can tell, are not intimately mixed with each other (Glotch et al., 2016).

Several previous works have characterized terrestrial playa evaporite minerals using VNIR reflectance spectra (Baldrige et al., 2004; Crowley, 1991; Eastes, 1989; Lynch et al., 2015). The bulk spectra of the playa minerals are dominated by carbonate, sulfate, and clay minerals. However, little work has been done with chloride-dominated mineral assemblages or with MIR emissivity spectra.

The goal of this laboratory work is to describe the VNIR reflectance and MIR emissivity spectral properties of multicomponent chloride salt-bearing mixtures. We focus on the spectral effects of varying abundances of evaporite and alteration minerals and particle sizes in mixtures with a chloride/silicate mixture. With these spectral characteristics, we constrain the detection limits of carbonate, sulfate, and phyllosilicate phases in salt/silicate mineral assemblages.

2. Samples and Methods

2.1. Sample Preparation

We use single minerals to focus only on the fundamental systematic investigation of chloride-bearing mixture spectra. The samples to be measured in this work are halite, labradorite, calcite, gypsum, nontronite, and mixtures thereof. All end-members were well characterized to assess the purity using a Rigaku Mini-Flex X-ray diffractometer from 10° to 70° 2θ at Department of Geosciences, Stony Brook University (Figure 1). Samples for X-ray diffraction analysis were ground powders with $<63\text{-}\mu\text{m}$ size fraction. Halite and labradorite were chosen for use in this study to make mixtures to represent the chloride-bearing deposits on Mars. Halite is the most likely form of chloride for the salt fraction of the chloride-bearing deposits on Mars (Glotch et al., 2016). We should clarify here that labradorite is not a direct analog for Martian basalt, but we use labradorite instead of basalt in this study not only based on geological and spectral consideration by Glotch et al. (2016) but also in order to avoid the complicating factors of other variables (e.g., many rock samples, although are better analog for the spectrum of the Martian basalt, have small amounts of minerals that have spectral features that obscure the focus of this study) to better isolate the effects of mineral composition abundance and particle size.

Calcite, gypsum, and nontronite were selected to represent the carbonate, sulfate, and phyllosilicate mineral groups, respectively. All samples were ground into powders using a mortar and pestle, and dry sieved to three size separates ($<10\ \mu\text{m}$, $63\text{--}90\ \mu\text{m}$, and $180\text{--}250\ \mu\text{m}$) as suggested by laboratory measurements and

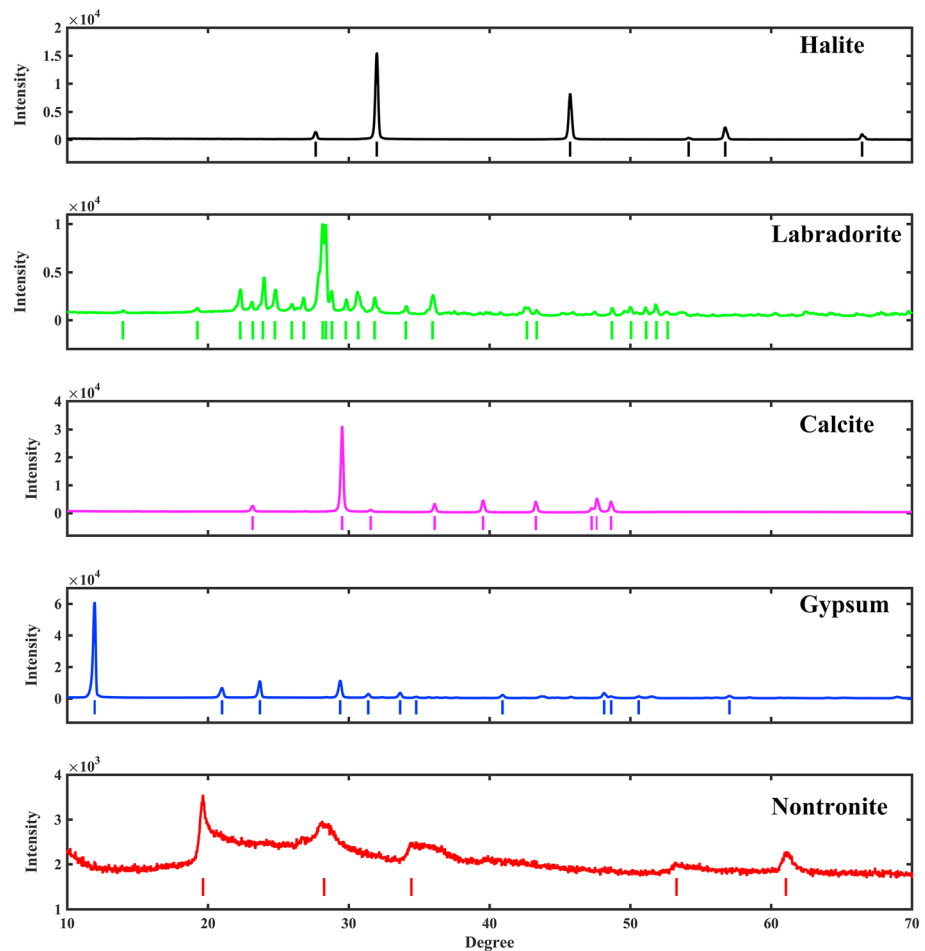


Figure 1. X-ray diffraction pattern for each end-member used in this study. Peaks in each X-ray diffraction pattern are confirmed by reference profile (e.g., halite: Walker et al., 2004; Labradorite: Wenk et al., 1980; calcite: Markgraf & Reeder, 1985; gypsum: Schofield et al., 1996; and nontronite: Che et al., 2011) showing ticks underneath each plot.

modeling constraints for grain sizes of salt-bearing deposits on Mars (Glotch et al., 2016). The <10- μm size fraction was separated in pure ethanol using Stokes' settling method (Day, 1965). The actual particle size distributions (Figure 2) were measured using a Malvern Mastersizer 2000 laser diffractometer available in the Department of Geosciences at Stony Brook University (Sperazza et al., 2004). We should note here the coarse size of nontronite due to the agglomeration of individual crystals, as clay mineral crystal sizes are typically very fine (<2 μm).

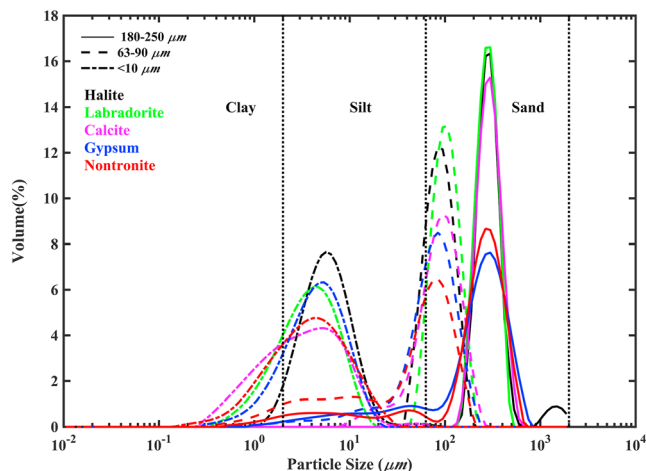


Figure 2. Particle size distribution of each end-member used in this study.

We prepared halite/labradorite mixtures, with either 10 or 20 wt% halite based on the constraints of Glotch et al. (2016). Then we kept the halite/labradorite mixture constant and documented the effects of varying minor mineral phases and their abundances on bulk spectral properties. To do this, a third component (either calcite, gypsum, or nontronite) was added until abundances of 0.1, 0.5, 1, 5, 10, and 20 wt% for each particle size were achieved.

2.2. Laboratory Spectral Measurements

VNIR (0.35–2.5 μm) bidirectional reflectance spectra were acquired at 1-nm spectral resolution using an ASD FieldSpec3 spectroradiometer at the Center for Planetary Exploration (CPEX), Stony Brook University.

Spectra of each sample were collected in the absence of ambient light with 30° and 0° incidence and emergence angles, respectively. All measurements were referenced to a calibrated Spectralon standard under identical conditions and corrected with Spectralon's absolute reflectance. Each spectrum was an average of 500 scans to provide enough signal-to-noise ratio. Each sample were run four times and then averaged to produce the final spectra.

MIR (2,000–225 cm^{-1} or 5 to ~ 44 μm) emissivity spectra were acquired at CPEX on a Nicolet 6700 FTIR spectrometer modified to collect emissivity spectra based on the method of Ruff et al. (1997). The spectrometer and the environment chamber were continuously purged with air from a purge gas generator scrubbed of CO_2 and H_2O . A blackbody heated to 70 and 100 °C was measured to derive the detector temperature and the instrument response function. Heated samples were maintained at 80 °C to provide adequate signal during the measurements. We note here that gypsum is able to dehydrate and become bassanite upon heating to 80 °C for several hours (Baldrige & Christensen, 2009), so in this work we only heat gypsum and mixtures with gypsum to 60 °C for only a short time (Figure S1 in the supporting information shows the VNIR reflectance spectra of gypsum before heating, after heating 2 hr at 60 °C and after heating overnight at 80 °C; Figure S2 shows the MIR emissivity spectra of gypsum after heating 2 hr at 60 °C and after heating overnight at 80 °C). A total of 256 scans of each sample were acquired at 4 cm^{-1} resolution using a CsI beamsplitter and an uncooled deuterated L-alanine doped triglycine sulfate (DLaTGS) detector and averaged to produce each spectrum. The acquired radiance spectrum was calibrated to spectral emissivity according to the method discussed in detail by Ruff et al. (1997). As mentioned by Glotch et al. (2016), when we calibrated the emissivity, we did not constrain the position of maximum brightness temperature, so our results do not have the overall blue slope as is seen in TES and THEMIS data of Martian chloride-bearing deposits.

3. Results

3.1. End-Members

VNIR reflectance and MIR emissivity spectral signatures of the mineral end-members used here and the spectral variation as a function of particle size have already been addressed by numerous previous studies (Adams & Goullaud, 1978; Bishop et al., 2008, 2014; Christensen et al., 2000; Cloutis et al., 2006; Farmer, 1974; Gaffey, 1986, 1987; Hunt, 1977; Hunt & Vincent, 1968; Lane, 2007; Lane & Christensen, 1997, 1998; Michalski et al., 2006; Mustard & Hays, 1997; Salisbury & Wald, 1992). The laboratory spectra of end-members with different size fractions we measured are illustrated in Figure 3. Here we summarize some dominant spectral properties of these end-members.

VNIR reflectance spectra of halite have high albedos and are featureless with the exception of a band at ~ 1.9 μm due to absorbed water on the sample. VNIR spectra of labradorite are characterized by a broad 1.25- μm absorption caused by Fe^{2+} in the crystal structure (Adams & Goullaud, 1978). Calcite shows absorption features at 1.9, 2.0, 2.16, 2.35, and 2.55 μm (cut at 2.5 μm here because of our instrument wavelength range) due to the overtones and combinations of fundamental vibration of C—O bonds (Gaffey, 1986, 1987). The gypsum bands at 1.0, 1.2, 1.4, 1.75, 1.9, 2.2, and 2.48 μm are attributed to the combinations and/or overtones of H_2O vibrational modes (Bishop et al., 2014; Cloutis et al., 2006). The major spectral features of nontronite are dominated by 0.5-, 0.68-, and 1- μm bands due to Fe electronic transitions, as well as OH stretching overtones at 1.4 μm , adsorbed and interlayer H_2O vibrational modes at 1.9 μm , and metal-OH deformation bands at 2.3 μm (Bishop et al., 2008). Overall, the VNIR reflectance spectra of our samples increase in reflectance with corresponding decreases in band contrast as the sample particle sizes are reduced.

MIR emissivity spectra of particulate minerals depend not only on the vibrations of the molecular structures but also on the variation of particle sizes. Generally speaking, band contrasts of the main absorption bands become weaker with the decrease of particle size. For the very fine particle size (< 10 μm), the fundamental vibrational features are nearly absent and transparency features, caused by sample volume scattering (Ito et al., 2018; Moersch & Christensen, 1995; Mustard & Hays, 1997; Salisbury & Wald, 1992), become prominent. MIR emissivity spectra of halite exhibit a low broad emissivity feature at higher frequencies and an upward slope toward lower frequencies to a maximum emissivity of unity at about 300 cm^{-1} . The peaks at $\sim 1,600$ and $\sim 1,120$ cm^{-1} in halite emissivity spectra are due to the minor contaminants of water and another phase, respectively (Lane & Christensen, 1998). The amount of contamination in

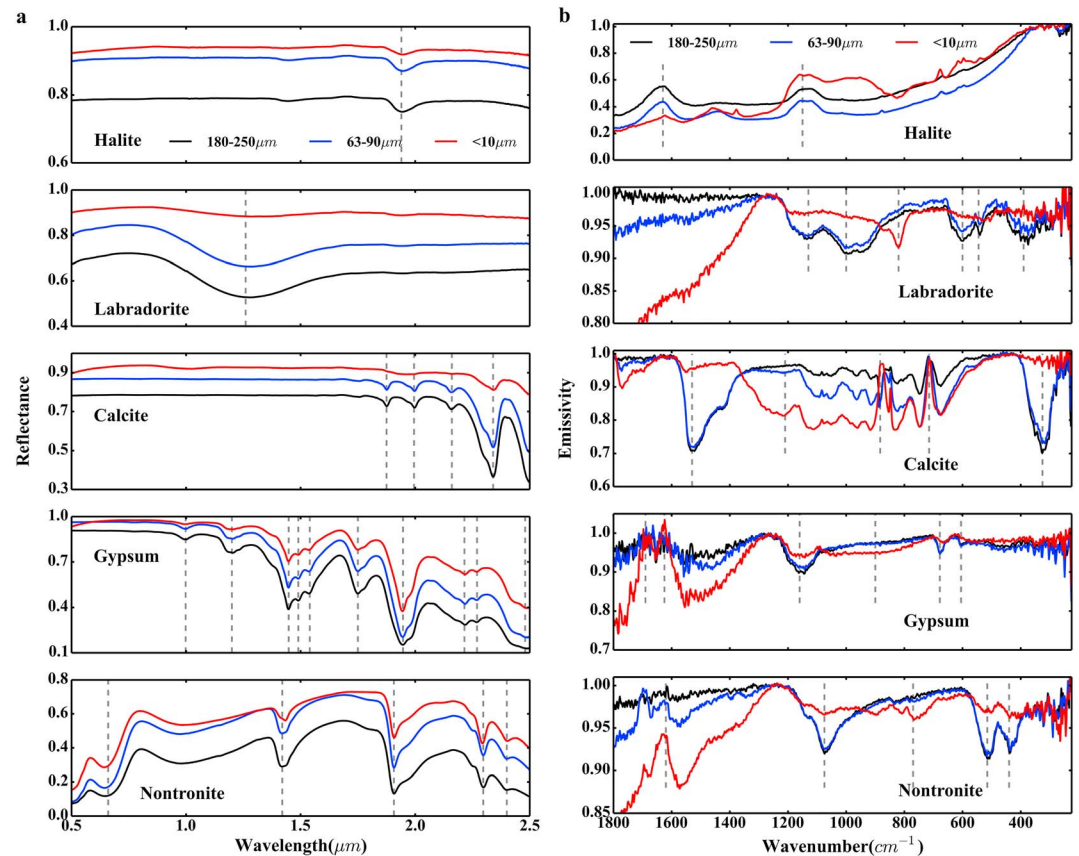


Figure 3. (a) Visible/near-infrared reflectance and (b) midinfrared emissivity of end-members for three different particle sizes used in this study.

halite is so low that it is not detectable from the X-ray diffraction pattern. Labradorite emissivity spectra display three main absorptions at $\sim 1,250\text{--}800\text{ cm}^{-1}$, $\sim 680\text{--}500\text{ cm}^{-1}$, and $\sim 500\text{--}300\text{ cm}^{-1}$ due to SiO_4 vibrations (Christensen et al., 2000). As particle size decreases, these three bands become weaker, while the transparency feature at $\sim 800\text{ cm}^{-1}$ develops. The calcite emissivity spectra show absorption features at approximately 1,550, 890, 715, and 300 cm^{-1} due to fundamental vibrations of C—O bonds (Lane & Christensen, 1997). Spectral features at about 1,150, 680, and 600 cm^{-1} of gypsum spectra are attributed to S—O bond oscillations (Lane, 2007). Nontronite shares similar band positions with those in labradorite due to SiO_4 vibrations but exhibits a more V-shaped band (Michalski et al., 2006). For $<10\text{-}\mu\text{m}$ size fraction, these vibrational bands are nearly obliterated and the transparency feature at the interband areas becomes dominant.

3.2. Two Component Mixtures

Spectra of halite and labradorite mixtures are shown in Figure 4. At VNIR wavelengths (Figure 4a), reflectance spectra of these samples have a broad absorption band at $\sim 1.25\text{ }\mu\text{m}$ attributed to Fe^{2+} in the labradorite. When the particle size is decreased, the overall reflectance is increased and band contrast is decreased. For each grain size fraction, the reflectance increases with the increased abundance of halite in the mixture.

At MIR wavelengths (Figure 4b), the emissivity spectra of halite/labradorite mixtures are dominated by labradorite spectral features. When halite is mixed with labradorite, all band contrast is reduced with the increased abundance of halite in the mixture. For the smallest size fraction, the Christiansen feature (CF), emissivity maximum, shifts from $\sim 1,250$ to $\sim 1,100\text{ cm}^{-1}$ when halite content is 20 wt% in the mixture.

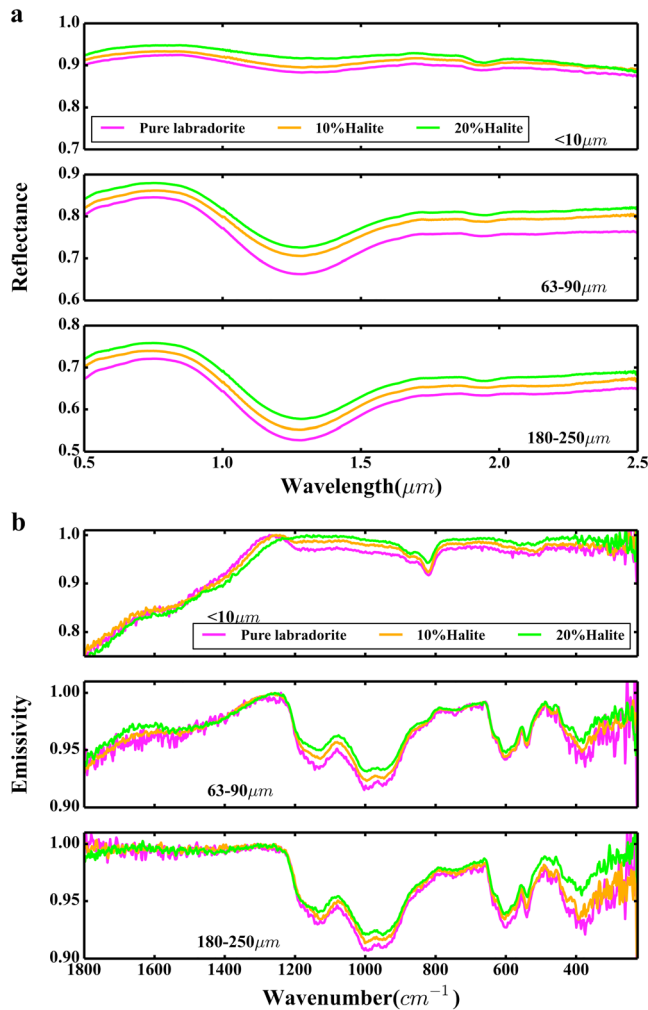


Figure 4. (a) Visible/near-infrared reflectance and (b) midinfrared emissivity spectra of halite and labradorite mixtures with 0%, 10%, and 20% halite; (top) $<10\text{-}\mu\text{m}$ size fraction, (middle) $63\text{-}90\text{ }\mu\text{m}$ size fraction, and (bottom) $180\text{-}250\text{ }\mu\text{m}$ size fraction.

3.3. Three Component Mixtures

3.3.1. VNIR Reflectance

VNIR reflectance spectra of halite/labradorite and calcite mixtures are shown in Figures 5a and 5b. The absorption bands associated with calcite at 2.35 and $2.5\text{ }\mu\text{m}$ in VNIR reflectance become more and more significant with the increased content of calcite into halite/labradorite mixture. The reflectance spectra of halite/labradorite mixtures with $0.1\text{-}1\text{ wt}\%$ calcite are dominated by the spectral feature of labradorite. With the addition of $5\text{ wt}\%$ and more calcite into halite/labradorite mixtures for the $180\text{-}250\text{ }\mu\text{m}$ and $63\text{-}90\text{ }\mu\text{m}$ size fractions, calcite absorption bands at 2.35 and $2.5\text{ }\mu\text{m}$ become more prominent. The $20\text{ wt}\%$ calcite mixtures show the minor absorption bands at 1.87 , 2 , and $2.15\text{ }\mu\text{m}$. For the $<10\text{-}\mu\text{m}$ size fraction, the calcite absorption bands do appear with high abundance of calcite ($>5\text{ wt}\%$) but show very small band contrast, no more than 2% .

Spectra of halite/labradorite and gypsum mixtures are shown in Figures 5c and 5d. The absorption bands attributed to gypsum at 1.4 , 1.75 , 1.9 , 2.2 , and $2.45\text{ }\mu\text{m}$ in VNIR spectra become stronger with the increased abundance of gypsum into the halite/labradorite mixture. For the $180\text{-}250\text{ }\mu\text{m}$ and $63\text{-}90\text{ }\mu\text{m}$ size fractions, when gypsum abundance is $5\text{ wt}\%$ or more, all of the gypsum absorption bands become prominent. These bands are much weaker in the $<10\text{-}\mu\text{m}$ size fraction compared with those in the coarser size fractions.

Spectra of halite/labradorite and nontronite mixtures are shown in Figures 5e and 5f. The VNIR reflectance decreases, and the absorption bands of nontronite at 0.5 , 0.68 , 1.0 , 1.4 , 1.9 , and $2.3\text{ }\mu\text{m}$ become well defined with increasing abundances of nontronite in the halite/labradorite mixtures.

3.3.2. MIR Emissivity

In the MIR wavelength region, the emissivity spectra are dominated by spectral features of labradorite when calcite abundance is lower than $5\text{ wt}\%$ (Figures 6a and 6b). At $5\text{ wt}\%$ and more calcite content, a band centered at $\sim 1,540\text{ cm}^{-1}$ appears gradually and the $\sim 300\text{ cm}^{-1}$ band becomes deeper and shifts to lower frequencies for the $180\text{-}250\text{ }\mu\text{m}$ and $63\text{-}90\text{ }\mu\text{m}$ size fractions. Some weak features located between 900 and 700 cm^{-1} start to appear when calcite abundance is $20\text{ wt}\%$. The $<10\text{-}\mu\text{m}$ size fraction

mixture, as expected, has a different spectral behavior compared to coarse size fractions. The emissivity spectra display transparency features at $\sim 1,300$ and $\sim 1,800\text{ cm}^{-1}$ when calcite abundance is at $5\text{ wt}\%$ or higher. Also, these two bands become stronger and the emissivity minimum of $\sim 1,300\text{ cm}^{-1}$ band shifts to lower frequencies with increased abundance of calcite. For the smallest size fraction, the 10% halite/ 90% labradorite mixture has a different CF position compared to the 20% halite/ 80% labradorite mixture as we mentioned above in the two-component mixtures. With the addition of calcite into halite/labradorite mixtures, the CF position of 10% halite/ 90% labradorite shifts to lower frequencies when calcite abundance is $5\text{ wt}\%$ or more, while the CF region of 20% halite/ 80% labradorite remains at the same position.

At MIR wavelengths, the main absorption band of gypsum for the $180\text{-}250\text{ }\mu\text{m}$ and $63\text{-}90\text{ }\mu\text{m}$ size fractions occurs at $\sim 1,160\text{ cm}^{-1}$, is located within the broad band of labradorite between $1,200$ and 800 cm^{-1} , and displays two small bands with emissivity minima at $\sim 1,150$ and $\sim 1,000\text{ cm}^{-1}$ (Figures 6c and 6d). Increasing abundances of gypsum in the halite/labradorite mixtures deepens the $1,150\text{ cm}^{-1}$ band contrast and weakens the $1,000\text{ cm}^{-1}$ band contrast simultaneously. The 10 and $20\text{ wt}\%$ gypsum mixtures show minor absorption bands at 730 cm^{-1} and also display two water peaks at $\sim 1,600$ and $\sim 1,700\text{ cm}^{-1}$ for $63\text{-}90\text{ }\mu\text{m}$ size fraction. For the $<10\text{-}\mu\text{m}$ size fraction, the water peaks at $\sim 1,600$ and $\sim 1,700\text{ cm}^{-1}$ start to appear with gypsum abundance at only $1\text{ wt}\%$ and become more prominent at $5\text{ wt}\%$ or more gypsum in the

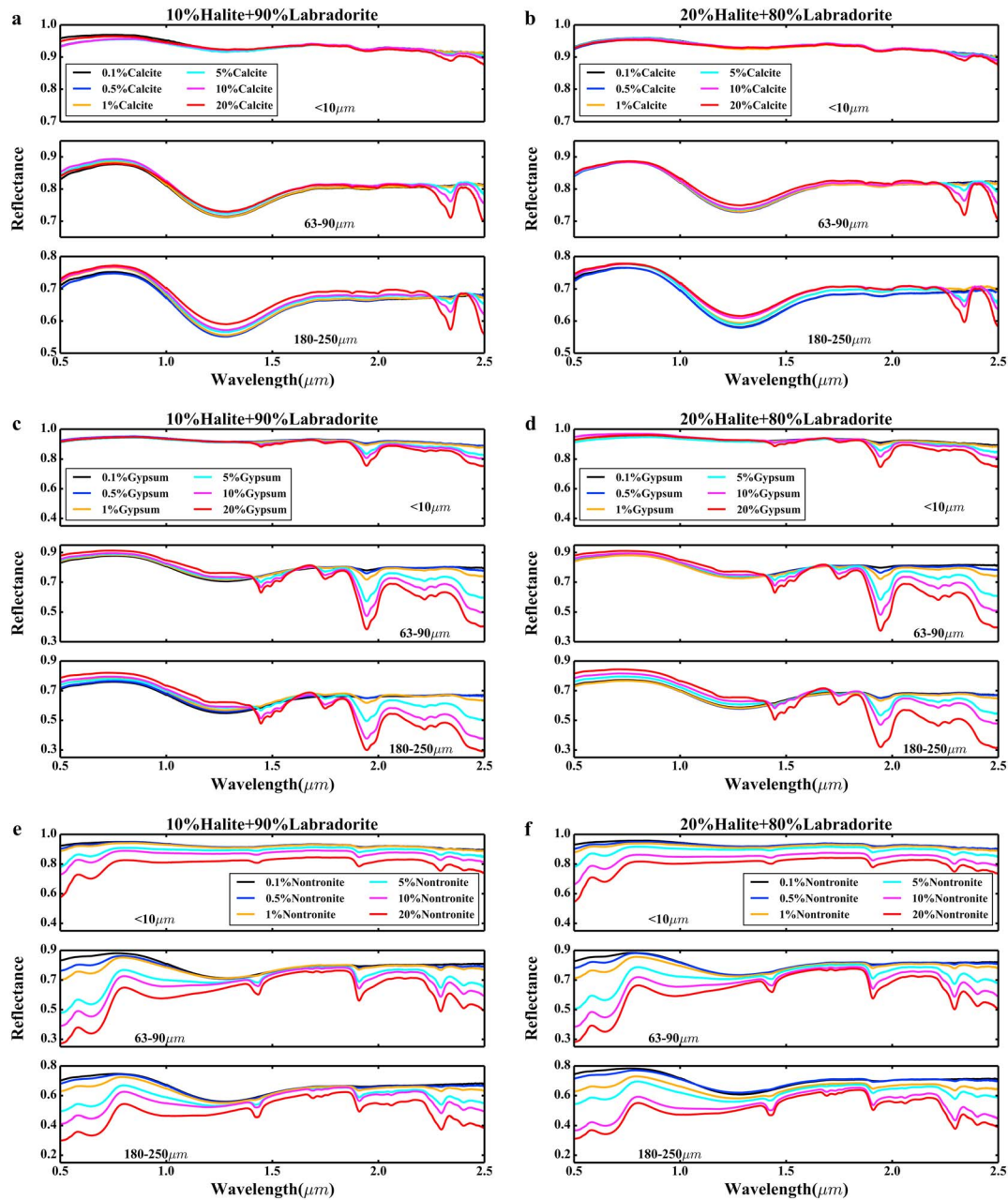


Figure 5. Visible/near-infrared reflectance spectra of halite/labradorite-third component mixtures. The left rows are 10%halite/90%labradorite mixtures with (a) calcite, (c) gypsum, and (e) nontronite. The right rows are 20%halite/80%labradorite mixtures with (b) calcite, (d) gypsum, and (f) nontronite. In each subplot, top is $<10\ \mu\text{m}$ size fraction, middle is $63\text{--}90\ \mu\text{m}$ size fraction, and bottom is $180\text{--}250\ \mu\text{m}$ size fraction.

mixtures. The CF position of 10%halite/90%labradorite stays at the same position regardless of the gypsum content change, whereas the CF region of 20%halite/80%labradorite shifts to higher frequencies when gypsum abundance is 5 wt% or more.

Emissivity spectra do not display significant changes with increasing abundances of nontronite in halite/labradorite mixtures because nontronite bands substantially overlap with those of labradorite in the MIR region (Figures 6e and 6f). However, with more than 5 wt% of nontronite in the halite/labradorite mixture, the silicate absorption band at $1,200\text{--}800\ \text{cm}^{-1}$ becomes narrower. For the $<10\text{-}\mu\text{m}$ size fraction, spectra of 5 wt% or more nontronite display the water peak at $\sim 1,600\ \text{cm}^{-1}$. The shift of CF position with abundance is similar to that seen in the gypsum mixtures. The CF position of 10%halite/90%labradorite

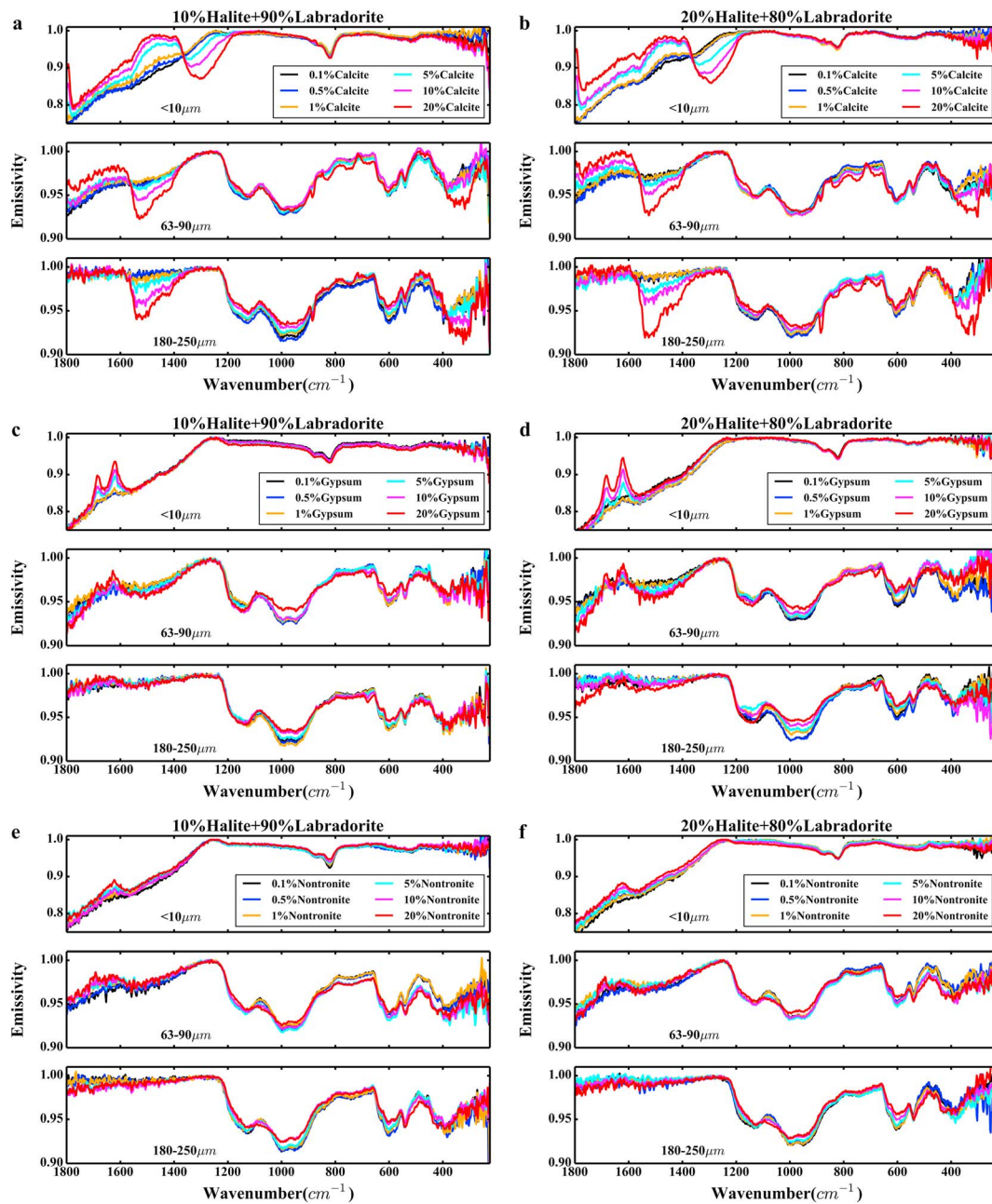


Figure 6. Midinfrared emissivity spectra of halite/labradorite-third component mixtures. The left rows are 10%halite/90%labradorite mixtures with (a) calcite, (c) gypsum, and (e) nontronite. The right rows are 20%halite/80%labradorite mixtures with (b) calcite, (d) gypsum, and (f) nontronite. In each subplot, top is $<10\ \mu\text{m}$ size fraction, middle is $63\text{--}90\ \mu\text{m}$ size fraction, and bottom is $180\text{--}250\ \mu\text{m}$ size fraction.

does not change with the nontronite concentration, while the CF region of 20%halite/80%labradorite shifts to higher frequencies when nontronite content is higher than 5 wt%.

4. Discussion

4.1. Spectral Trends

The laboratory work presented here shows that systematic variations in bulk spectral characteristics are clearly apparent as the concentrations of minor minerals and particle sizes are varied in the halite/labradorite mixtures.

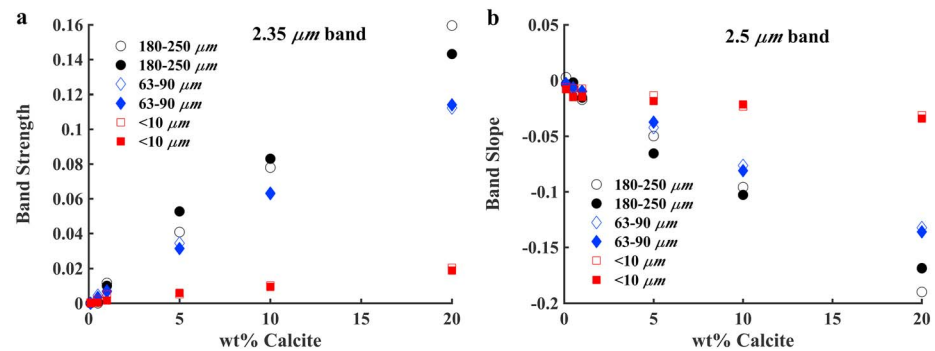


Figure 7. (a) Band strength of 2.35- μm absorption band and (b) slope between 2.4 and 2.5 μm vs. abundances of calcite in halite/labradorite mixtures in visible/near-infrared absolute reflectance spectra. The black circle symbols represent 180–250 μm size fraction, the blue diamond symbols represent 63–90 μm size fraction, and the red square symbols represent <10- μm size fraction. The filled symbols represent 10%halite/90%labradorite-calcite mixtures; the empty symbols represent 20%halite/80%labradorite-calcite mixtures.

4.1.1. VNIR Spectral Trends

In VNIR reflectance spectra within each ternary series, an increase in calcite, gypsum, or nontronite results in an increase in their respective absorption strengths for relatively coarse size fractions (180–250 μm and 63–90 μm). However, the reduced spectral contrasts in extremely fine-grained (<10 μm) samples make absorption features very weak.

Variation of VNIR spectral reflectance with composition can be better analyzed quantitatively using the band depth from the normalized reflectance of absorption bands (Clark, 1999). The purpose of parameterizing the laboratory data here is to better clarify the systematic spectral changes produced by varying end-member abundance beyond what is visually apparent. For the ternary mixture with calcite (Figure 7), the 2.35- μm band strength increases monotonically with the calcite abundance in the mixture. The 2.5- μm band is not completely resolved because the measurement range ends at 2.5 μm , so instead we calculated the slope between 2.4 and 2.5 μm . The 180–250 μm and 63–90 μm size fractions have steep slopes compared with <10- μm size fraction. The plots of band depth versus gypsum content (Figure 8) show trends similar to that seen with calcite: a monotonic increase of band strength with the addition of gypsum abundance. Band depths of two coarse size fractions increase faster than those for <10- μm size fraction. For the nontronite mixture (Figure 9), the OH vibrational bands display trend similar to those seen for calcite and gypsum. However, the Fe electronic transition bands at 0.5 and 0.68 μm remain similar for all particle sizes. The smaller size fractions even have deeper bands in some cases.

Parameterization of band depth versus phase abundance quantifies how variation in the concentration of minor phase in the halite/labradorite mixture affects changes in the overall reflectance spectrum of the mixture. These observations illustrate that evaporite minerals and weathering products we tested here strongly influence spectra of particulate mixtures in which small changes in concentration display large changes in bulk spectral properties and can dominate the spectra even at very low abundances.

4.1.2. MIR Spectral Trends

MIR emissivity spectra display systematic changes in overall spectral properties with the proportion of the third component in the halite/labradorite mixtures. We see that the diagnostic band features of individual minerals become significant according to the weight percentage of the third component. For example, the calcite absorption band at $\sim 1,530\text{ cm}^{-1}$ for coarse particle sizes (180–250 μm and 63–90 μm) and the $\sim 1,300\text{ cm}^{-1}$ transparency feature for the smallest size fraction (<10 μm), as well as the water peak feature found in the <10- μm gypsum and nontronite spectra, are clear evidence of spectral trends according to the composition abundance variation.

In addition to the particular band for each mineral, we note that there are some other parameters that can be used to characterize the spectral change. Although the gypsum diagnostic band ($1,160\text{ cm}^{-1}$) is located inside the broad band of labradorite ($1,250\text{--}800\text{ cm}^{-1}$), which makes spectral changes somewhat difficult to evaluate, we can calculate the slope between the emissivity values at $1,160$ and $1,000\text{ cm}^{-1}$ to quantify

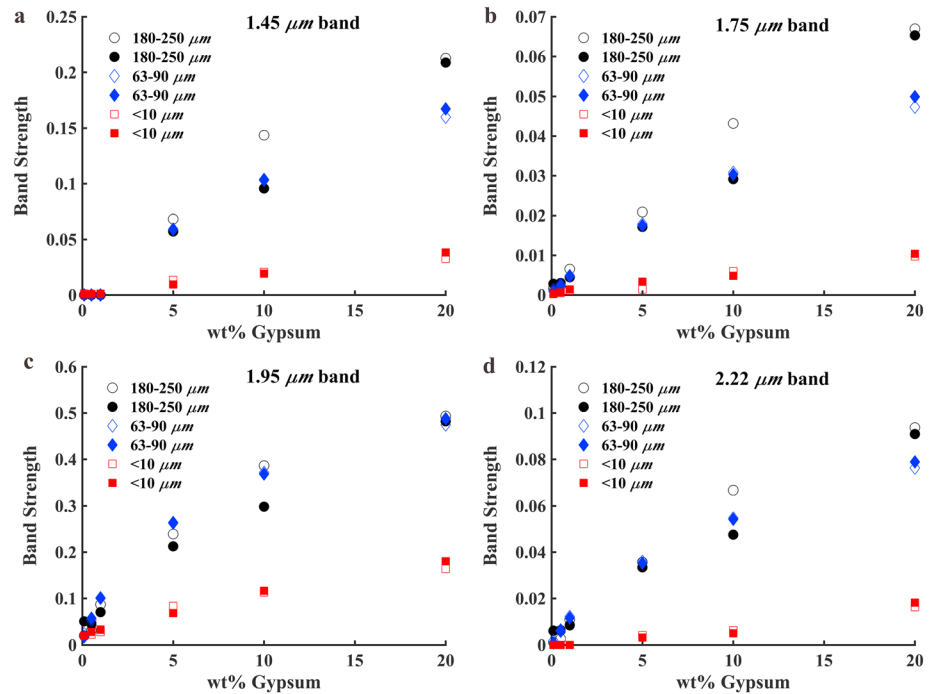


Figure 8. Band strength of (a) 1.45- μm absorption band, (b) 1.75 μm absorption band, (c) 1.95- μm absorption band c, (d) 2.22- μm absorption band vs. abundances of gypsum in halite/labradorite mixtures in visible/near-infrared absolute reflectance spectra. The black circle symbols represent 180–250 μm size fraction, the blue diamond symbols represent 63–90 μm size fraction, and the red square symbols represent <10- μm size fraction. The filled symbols represent 10%halite/90%labradorite-calcite mixtures; the empty symbols represent 20%halite/80%labradorite-calcite mixtures.

the effect of gypsum concentration on the bulk spectra of mixture. Figure 10 shows that slope changes from negative to positive as gypsum concentrations increase. The nontronite-bearing mixtures are another case in which overlapping band positions complicate the assessment of spectral trends. However, with increasing abundances of nontronite present in the halite/labradorite mixtures, the silicate absorption band at 1,250–800 cm^{-1} changes shape as the peak between two small bands at 1,250–800 cm^{-1} becomes lower and the region displays a V shape, which is similar to Martian surface type 2 spectra (Bandfield et al., 2000; Wyatt & McSween, 2002).

Finally, the CF position in the very fine particle size fraction (<10 μm) samples is also an important indicator of spectral variation. The halite concentration has a significant effect on the MIR spectra of the smallest size fractions. For the <10- μm size fractions, samples with 20 wt% halite show a shift of the CF position from $\sim 1,250$ to $\sim 1,100$ cm^{-1} compared to samples with 10 wt% halite. This behavior is similar to that of the new chloride spectral shape identified in dusty regions of Mars by Glotch et al. (2016). When we mix fine particulate halite/labradorite with calcite, gypsum, and nontronite, respectively, the corresponding CF position change is summarized in Table 1.

We note that both VNIR reflectance and MIR emissivity spectra of our ternary mixtures display complementary systematic variations with changes in minor phase concentration. For instance, if VNIR reflectance is not sensitive enough to detect the absorptions of individual minerals from the finest size fractions, we can examine emissivity spectra to trace transparency features, water peaks, and CF positions to help constrain the mineral detection. On the other hand, spectral trends of gypsum- and nontronite-bearing ternary mixtures can be more difficult to detect in emissivity spectra, whereas there trend to be clear patterns of band depth changes in VNIR reflectance spectra.

4.2. Minor Phase Detection Limits

The laboratory spectral observations of chloride-salt bearing assemblages show that minor phases including the evaporite minerals and phyllosilicates we tested here could be clearly detected at low abundance in chloride/silicate mixtures in both VNIR reflectance and MIR emissivity spectra.

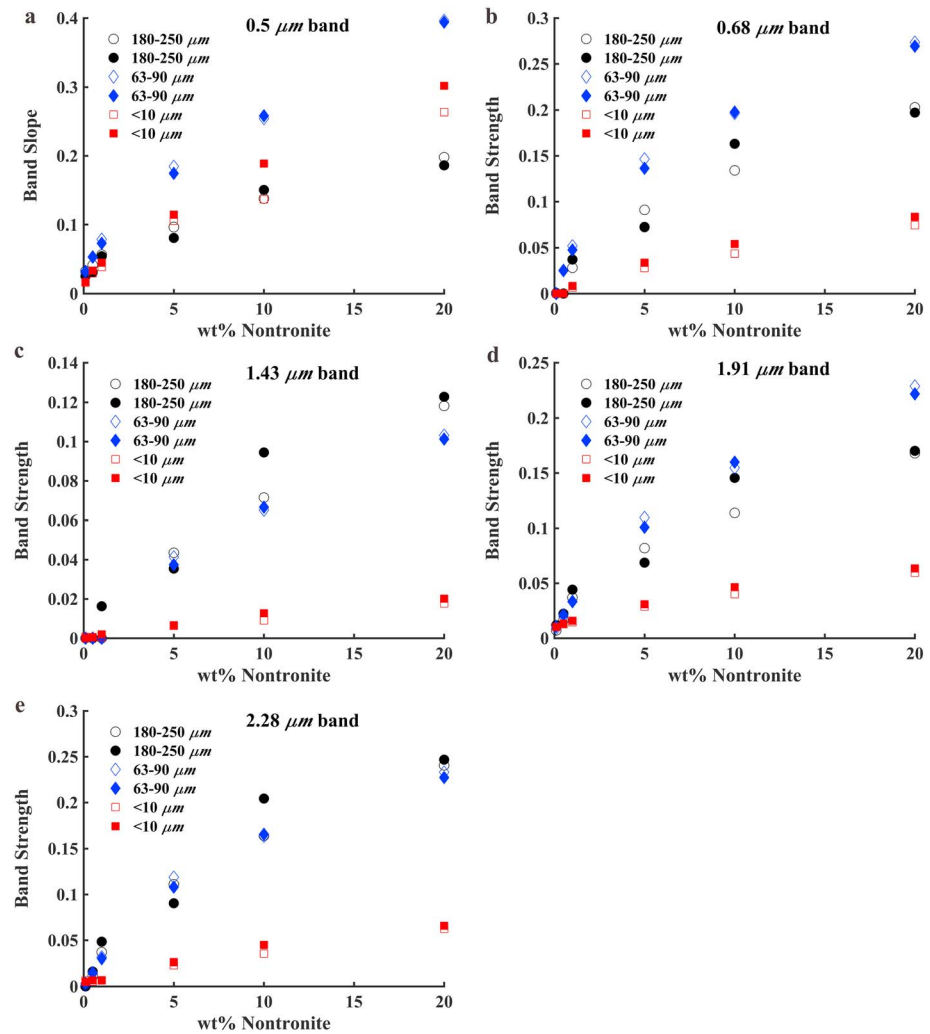


Figure 9. (a) Band slope between 0.5 and 0.6- μm region, (b) band strength of 0.68- μm absorption band, (c) 1.43- μm absorption band, (d) 1.91 μm absorption band, and (e) 2.28- μm absorption band vs. abundances of nontronite in halite/labradorite mixtures in visible/near-infrared absolute reflectance spectra. The black circle symbols represent 180–250 μm size fraction, the blue diamond symbols represent 63–90 μm size fraction, and the red square symbols represent <10- μm size fraction. The filled symbols represent 10%halite/90%labradorite-calcite mixtures; the empty symbols represent 20%halite/80%labradorite-calcite mixtures.

The VNIR reflectance spectra were quantitatively analyzed for the presence of diagnostic absorption bands of individual minor phase by calculating the band strength (Figure 7) to help constrain the detection limits of these extra components in the chloride/silicate mixture. In most cases, 1–2% band depth can be detected in reflectance spectra (Lynch et al., 2015). The MIR emissivity spectra can be quantitatively characterized by the minimum or maximum value of the typical features as well as CF position. We should emphasize here that the emissivity measurement methods we used are accurate in most cases to within 1–2% (Ruff et al., 1997).

Calcite has typical diagnostic absorption bands, including 2.35- μm band and 2.5- μm shoulder, as well as $\sim 1,560\text{ cm}^{-1}$ absorption band in the VNIR and MIR wavelength ranges, respectively. From the band strength plot in VNIR wavelengths and band minimum value in MIR emissivity, we can see that 5 wt% or more calcite is needed to increase the band depth to larger than 2% in VNIR reflectance and result in a significant band minimum change significant in MIR emissivity for coarse size fractions (180–250 μm and 63–90 μm). Although the 2.35- and 2.5- μm band depths are too weak (<2% even with 20 wt% calcite) for smallest size fraction (<10 μm) in VNIR reflectance spectra, the transparency feature

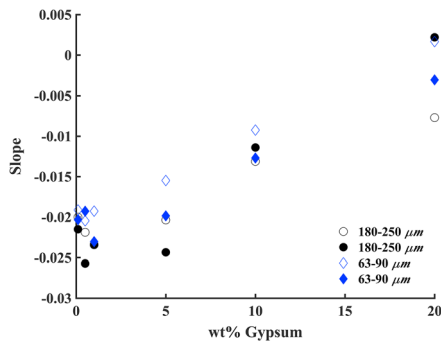


Figure 10. Calculated slopes between 1,160 and 1,000 cm^{-1} vs. abundances of gypsum in halite/labradorite mixtures for two coarse size fractions. The black circle symbols represent 180–250 μm size fraction; the blue diamond symbols represent 63–90 μm size fraction. The filled symbols represent 10%halite/90%labradorite-gypsum mixtures; the empty symbols represent 20%halite/80%labradorite-gypsum mixtures.

at $\sim 1,300 \text{ cm}^{-1}$, in addition to the CF position change in MIR emissivity spectra within the 10%halite/90%labradorite mixture, indicate the clear detection of calcite in finely particulate chloride mixtures require at least 5 wt% calcite.

Gypsum has a variety of absorption bands at VNIR wavelengths and several features in the MIR wavelength range. Of those, the 1.9- μm band is the strongest band of gypsum; however, it also can be caused by adsorbed water in the sample without gypsum. As a result, this band can obscure the detection limit of hydrated minerals. The 1.4- μm triplet, 1.75- and 2.26- μm bands are principal features of gypsum, which are used here to clearly constrain that the existence of gypsum at 5 wt% can be detected in VNIR reflectance spectra of ternary mixtures. While the slope we developed between 1,160 and 1,000 cm^{-1} can be used to characterize the spectral change, it is not a great parameter to define a detection limit without a standard criterion. For the finest size fraction, the water peak at $\sim 1,600 \text{ cm}^{-1}$ and CF position change reveal that 5 wt% of gypsum can be distinguishable from the chloride/silicate mixtures.

For nontronite, Fe electronic transition bands at 0.5, 0.68, and 1 μm can be identified when at 1 wt% nontronite concentrations, while the OH combination vibration bands at 1.4, 1.9, and 2.3 μm are easily detected at 5 wt% nontronite. In the MIR region, the $\sim 1,600 \text{ cm}^{-1}$ water peak and CF position shift for finest particle size suggest that the detection limit of nontronite is 5 wt%. Together, for the chloride-bearing mixtures we explored here, those containing >1–5 wt% minor phases generally can be identified from the chloride/silicate mixtures.

4.3. Implication for Mars

While the laboratory spectroscopy of chloride-bearing assemblages characterized in this study should not be considered a direct comparison to remotely measured Martian chloride-bearing units at this stage, they are selected to facilitate a fundamental investigation of spectral properties that arise solely

from variations of mineral composition and particle size, without complexities from other variables. The laboratory spectral analyses here provide a systematic framework for estimating the concentrations of other minor phases that could be *hidden* in the VNIR and MIR spectra of Martian chloride-bearing terrains. The results suggest that evaporite minerals and weathering products are generally distinguishable from chloride-bearing deposits even when present in very small concentrations.

Even though the low presence of minor phases in chloride salt-bearing assemblages constrained in this study might be controversial with the evaporative environment formation mechanism of chloride salt on Mars, the textural differences from actual Martian chloride-bearing deposits impede exact quantification of mineral abundances at this time. One explanation is that other evaporite phases of alteration products are just buried by chloride-bearing deposits and remain undetectable. Laboratory work by Berger et al. (2015) has illustrated that halite coating thickness and texture can be important factors to affect the spectral signatures of materials underneath at MIR wavelengths. Their work has shown that continuous and coarse particulate halite coating with >150- μm thickness can obscure the substrate spectral signatures, although this has yet to be verified at VNIR wavelengths. Future studies should build upon the foundations provided by this simplified laboratory data set to more closely estimate the comprehensive characteristics of Martian chloride salts.

Table 1
Christiansen Feature Positions for Ternary Compositions for the <10- μm Size Fraction

End-member	10%Halite/ 90%Labradorite CF position (cm^{-1})	20%Halite/ 90%Labradorite CF position (cm^{-1})
0.1% calcite	1,245	1,090
0.5% calcite	1,245	1,090
1% calcite	1,245	1,090
5% calcite	1,085	1,090
10% calcite	1,085	1,090
20% calcite	1,085	1,090
0.1% gypsum	1,245	1,090
0.5% gypsum	1,245	1,090
1% gypsum	1,245	1,090
5% gypsum	1,245	1,150
10% gypsum	1,245	1,150
20% gypsum	1,245	1,150
0.1% nontronite	1,250	1,078
0.5% nontronite	1,250	1,080
1% nontronite	1,250	1,080
5% nontronite	1,250	1,240
10% nontronite	1,250	1,240
20% nontronite	1,250	1,240

5. Conclusions

Remote sensing measurements suggest that chlorides on Mars are two component mixtures of chloride salt and the regional basalt regolith without any other minor minerals that might typically be found in evaporite or chemical weathering environments. This study has been designed to document the various effects of composition, abundance, and particle size of calcite, gypsum, and nontronite on VNIR reflectance and MIR emissivity spectra of chloride-bearing mixtures.

Spectral characteristics of chloride salts are readily overwhelmed by the spectral contributions of other evaporite minerals and alteration products even though they are less abundant than the chlorides. Both VNIR reflectance and MIR emissivity spectral features indicate that >1–5% relative mass fraction of minor phase in the salt-assemblages result in spectra that cannot be the same as the halite/labradorite mixture and therefore can be detected.

While the well-controlled, systematic data set produced here provides a framework for developing applications to more complex remotely acquired spectra from the Martian surface, several other factors such as physical textures (e.g., halite coating) of chloride-bearing mixtures besides intimate mixing need to be tested. In addition to the strictly controlled laboratory experiments, the validation of theoretical spectroscopic modeling approaches would provide leverage for continuing to investigate more complex set of conditions that characterize Martian chloride-bearing deposits.

Acknowledgments

This work was supported by NASA Solar System Workings award NNX15AL55G to T. D. Glotch. All laboratory spectral data will be archived at the Stony Brook University Academic Commons repository (<https://commons.library.stonybrook.edu/geodata/5>). We are grateful to Darby Dyar for providing mineral sample of labradorite. We are also grateful to Carey Legett and Katherine Shirley for helpful discussions as well as Gen Ito for his informal review of this manuscript. We thank Edward Cloutis and an anonymous reviewer for constructive and thorough reviews. We also thank Editor Steve Hauck for helpful suggestions that improve the clarity of the manuscript.

References

- Adams, J. B., & Goullaud L. H. (1978). Plagioclase feldspars: Visible and near infrared diffuse reflectance spectra as applied to remote sensing. *Proc. Lunar Planet. Sci. Conf.*, 9th, 2901–1909.
- Baldrige, A. M., & Christensen, P. R. (2009). A laboratory technique for thermal emission measurement of hydrated minerals. *Applied Spectroscopy*, 63(6), 678–688. <https://doi.org/10.1366/000370209788559665>
- Baldrige, A. M., Farmer, J. D., & Moersch, J. E. (2004). Mars remote-sensing analog studies in the Badwater Basin, Death Valley, California. *Journal of Geophysical Research*, 109, E12006. <https://doi.org/10.1029/2004JE002315>
- Bandfield, J. L., Hamilton, V. E., & Christensen, P. R. (2000). A global view of Martian surface compositions from MGS-TES. *Science*, 287(5458), 1626–1630. <https://doi.org/10.1126/science.287.5458.1626>
- Berger, J. A., King, P. L., Green, A., Craig, M. A., Spilde, M. N., Wright, S. P., et al. (2015). Effect of halite coatings on thermal infrared spectra. *Journal of Geophysical Research: Solid Earth*, 120, 2162–2178. <https://doi.org/10.1002/2014JB011712>
- Bishop, J. L., Lane, M. D., Dyar, M. D., & Brown, A. J. (2008). Reflectance and emission spectroscopy study of four groups of phyllosilicates: Smectites, kaolinite-serpentines, chlorites and micas. *Clay Minerals*, 43(1), 35–54. <https://doi.org/10.1180/claymin.2008.043.1.03>
- Bishop, J. L., Lane, M. D., Dyar, M. D., King, S. J., Brown, A. J., & Swayze, G. A. (2014). Spectral properties of Ca-sulfates: Gypsum, bassanite, and anhydrite. *American Mineralogist*, 99(10), 2105–2115. <https://doi.org/10.2138/am-2014-4756>
- Che, C., Glotch, T. D., Bish, D. L., Michalski, J. R., & Xu, W. (2011). Spectroscopic study of the dehydration and dehydroxylation of phyllosilicate and zeolite minerals. *Journal of Geophysical Research*, 116, E05007. <https://doi.org/10.1029/2010JE003740>
- Christensen, P. R., Bandfield, J. L., Hamilton, V. E., Howard, D. A., Lane, M. D., Piatek, J. L., et al. (2000). A thermal emission spectral library of rock-forming minerals. *Journal of Geophysical Research*, 105(E4), 9735–9739. <https://doi.org/10.1029/1998JE000624>
- Clark, R. N. (1999). Spectroscopy of rocks and minerals, and principles of spectroscopy. In A. N. Rencz (Ed.), *Manual of remote sensing, remote sensing for the Earth sciences* (Vol. 3, chap. 1, pp. 3–58). New York: John Wiley.
- Cloutis, E. A., Hawthorne, F. C., Mertzman, S. A., Krenn, K., Craig, M. A., Marcino, D., et al. (2006). Detection and discrimination of sulfate minerals using reflectance spectroscopy. *Icarus*, 184(1), 121–157. <https://doi.org/10.1016/j.icarus.2006.04.003>
- Crowley, J. K. (1991). Visible and near-infrared (0.4–2.5 μm) reflectance spectra of playa evaporite minerals. *Journal of Geophysical Research*, 96(B10), 16,231–16,240. <https://doi.org/10.1029/91JB01714>
- Day, P. R. (1965). Particle fractionation and particle-size analysis. In C. A. Black et al. (Eds.), *Methods of Soil Analysis, Part 1: Physical and Mineralogical Properties, Including Statistics of Measurement and Sampling* (pp. 545–567). Madison, WI: American Society of Agronomy.
- Eastes, J. W. (1989). Spectral properties of halite-rich mineral mixtures: Implications for middle infrared remote-sensing of highly saline environments. *Remote Sensing of Environment*, 27(3), 289–303. [https://doi.org/10.1016/0034-4257\(89\)90089-8](https://doi.org/10.1016/0034-4257(89)90089-8)
- El-Maarry, M. R., Pommerol, A., & Thomas, N. (2013). Analysis of polygonal cracking patterns in chloride-bearing terrains on Mars: Indicators of ancient playa settings. *Journal of Geophysical Research: Planets*, 118, 2263–2278. <https://doi.org/10.1002/2013JE004463>
- El-Maarry, M. R., Watters, W., McKeown, N. K., Carter, J., Dobrea, E. N., Bishop, J. L., Pommerol, A., et al. (2014). Potential desiccation cracks on Mars: A synthesis from modeling, analogue-field studies, and global observations. *Icarus*, 241, 248–268. <https://doi.org/10.1016/j.icarus.2014.06.033>
- Eugster, H. P., & Hardie, L. A. (1978). Saline lakes. In A. Lerman (Ed.), *Lakes: Chemistry, geology, physics* (pp. 237–293). New York: Springer. https://doi.org/10.1007/978-1-4757-1152-3_8
- Farmer, V. C. (1974). In V. C. Farmer (Ed.), *The infrared spectra of minerals*. London: Mineralogical Society. <https://doi.org/10.1180/mono-4>
- Gaffey, S. J. (1986). Spectral reflectance of carbonate minerals in the visible and near-infrared (0.35–2.55 μm): Calcite, aragonite, and dolomite. *American Mineralogist*, 71(1–2), 151–162.
- Gaffey, S. J. (1987). Spectral reflectance of carbonate minerals in the visible and near-infrared (0.35–2.55 μm): Anhydrous carbonate minerals. *Journal of Geophysical Research*, 92(B2), 1429–1440. <https://doi.org/10.1029/JB092iB02p01429>
- Glotch, T. D., Bandfield, J. L., Tornabene, L. L., Jensen, H. B., & Seelos, F. P. (2010). Distribution and formation of chlorides and phyllosilicates in Terra Sirenum, Mars. *Geophysical Research Letters*, 37, L16202. <https://doi.org/10.1029/2010GL044557>

- Glotch, T. D., Bandfield, J. L., Wolff, M. J., Arnold, J. A., & Che, C. C. (2016). Constraints on the composition and particle size of chloride salt-bearing deposits on Mars. *Journal of Geophysical Research: Planets*, *121*, 454–471. <https://doi.org/10.1002/2015JE004921>
- Glotch, T. D., Phillips B. P., Bandfield J. L., Osterloo M. M., & Rogers A. D. (2017). The hydration state of chloride salt deposits on Mars. 48th Lunar and Planetary Science Conference, 2232.
- Hunt, G. R. (1977). Spectral signatures of particulate minerals in visible and near infrared. *Geophysics*, *42*(3), 501–513. <https://doi.org/10.1190/1.1440721>
- Hunt, G. R., & Vincent, R. K. (1968). Behavior of spectral features in infrared emission from particulate surfaces of various grain sizes. *Journal of Geophysical Research*, *73*(18), 6039–6046. <https://doi.org/10.1029/JB073i018p06039>
- Hynek, B. M., Osterloo, M. K., & Kierein-Young, K. S. (2015). Late-stage formation of Martian chloride salts through ponding and evaporation. *Geology*, *43*(9), 787–790. <https://doi.org/10.1130/G36895.1>
- Ito, G., Mishchenko, M. I., & Glotch, T. D. (2018). Radiative-transfer modeling of spectra of planetary regoliths using cluster-based dense packing modifications. *Journal of Geophysical Research: Planets*, *123*, 1203–1220. <https://doi.org/10.1029/2018JE005532>
- Jensen, H. B., & Glotch, T. D. (2011). Investigation of the near-infrared spectral character of putative Martian chloride deposits. *Journal of Geophysical Research*, *116*, E00J03. <https://doi.org/10.1029/2011JE003887>
- Lane, M. D. (2007). Mid-infrared emission spectroscopy of sulfate and sulfate-bearing minerals. *American Mineralogist*, *92*(1), 1–18. <https://doi.org/10.2138/am.2007.2170>
- Lane, M. D., & Christensen, P. R. (1997). Thermal infrared emission spectroscopy of anhydrous carbonates. *Journal of Geophysical Research*, *102*(E11), 25,581–25,592. <https://doi.org/10.1029/97JE02046>
- Lane, M. D., & Christensen, P. R. (1998). Thermal infrared emission spectroscopy of salt minerals predicted for Mars. *Icarus*, *135*(2), 528–536. <https://doi.org/10.1006/icar.1998.5998>
- Lynch, K. L., Horgan, B. H., Munakata-Marr, J., Hanley, J., Schneider, R. J., Rey, K. A., et al. (2015). Near-infrared spectroscopy of lacustrine sediments in the Great Salt Lake Desert: An analog study for Martian paleolake basins. *Journal of Geophysical Research: Planets*, *120*, 599–623. <https://doi.org/10.1002/2014JE004707>
- Markgraf, S. A., & Reeder, R. J. (1985). High-temperature structure refinements of calcite and magnesite. *American Mineralogist*, *70*, 590–600.
- Michalski, J. R., Kraft, M. D., Sharp, T. G., Williams, L. B., & Christensen, P. R. (2006). Emission spectroscopy of clay minerals and evidence for poorly crystalline aluminosilicates on Mars from Thermal Emission Spectrometer data. *Journal of Geophysical Research*, *111*, E03004. <https://doi.org/10.1029/2005JE002438>
- Moersch, J. E., & Christensen, P. R. (1995). Thermal emission from particulate surfaces: A comparison of scattering models with measured spectra. *Journal of Geophysical Research*, *100*(E4), 7465–7477. <https://doi.org/10.1029/94JE03330>
- Murchie, S. L., Mustard, J. F., Ehlmann, B. L., Milliken, R. E., Bishop, J. L., McKeown, N. K., et al. (2009). A synthesis of Martian aqueous mineralogy after 1 Mars year of observations from the Mars Reconnaissance Orbiter. *Journal of Geophysical Research*, *114*, E00D06. <https://doi.org/10.1029/2009JE003342>
- Mustard, J. F., & Hays, J. E. (1997). Effects of hyperfine particles on reflectance spectra from 0.3 to 25 μm . *Icarus*, *125*(1), 145–163. <https://doi.org/10.1006/icar.1996.5583>
- Osterloo, M. M., Anderson, F. S., Hamilton, V. E., & Hynek, B. M. (2010). Geologic context of proposed chloride-bearing materials on Mars. *Journal of Geophysical Research*, *115*, E10012. <https://doi.org/10.1029/2010JE003613>
- Osterloo, M. M., Hamilton, V. E., Bandfield, J. L., Glotch, T. D., Baldrige, A. M., Christensen, P. R., et al. (2008). Chloride-bearing materials in the southern highlands of Mars. *Science*, *319*(5870), 1651–1654. <https://doi.org/10.1126/science.1150690>
- Ruesch, O., Poulet, F., Vincendon, M., Bibring, J. P., Carter, J., Erkeling, G., et al. (2012). Compositional investigation of the proposed chloride-bearing materials on Mars using near-infrared orbital data from OMEGA/Mex. *Journal of Geophysical Research*, *117*, E00J13. <https://doi.org/10.1029/2012JE004108>
- Ruff, S. W., Christensen, P. R., Barbera, P. W., & Anderson, D. L. (1997). Quantitative thermal emission spectroscopy of minerals: A laboratory technique for measurement and calibration. *Journal of Geophysical Research*, *102*(B7), 14,899–14,913. <https://doi.org/10.1029/97JB00593>
- Salisbury, J. W., & Wald, A. (1992). The role of volume scattering in reducing spectral contrast of reststrahlen bands in spectra of powdered minerals. *Icarus*, *96*(1), 121–128. [https://doi.org/10.1016/0019-1035\(92\)90009-V](https://doi.org/10.1016/0019-1035(92)90009-V)
- Schofield, P. F., Knight, K. S., & Stretton, I. C. (1996). Thermal expansion of gypsum investigated by neutron powder diffraction. *American Mineralogist*, *81*(7-8), 847–851. <https://doi.org/10.2138/am-1996-7-807>
- Sperazza, M., Moore, J. N., & Hendrix, M. S. (2004). High-resolution particle size analysis of naturally occurring very fine-grained sediment through laser diffractometry. *Journal of Sedimentary Research*, *74*(5), 736–743. <https://doi.org/10.1306/031104740736>
- Tosca, N. J., & McLennan, S. M. (2006). Chemical divides and evaporite assemblages on Mars. *Earth and Planetary Science Letters*, *241*(1–2), 21–31. <https://doi.org/10.1016/j.epsl.2005.10.021>
- Walker, D., Verma, P. K., Cranswick, L. M. D., Jones, R. L., Clark, S. M., & Buhre, S. (2004). Halite-sylvite thermoelasticity. *American Mineralogist*, *89*(1), 204–210. <https://doi.org/10.2138/am-2004-0124>
- Wenk, H. R., Joswig, W., Tagai, T., Korekawa, M., & Smith, B. K. (1980). The average structure of An_{62-66} labradorite. *American Mineralogist*, *65*, 81–95.
- Wray, J. J., Murchie, S. L., Squyres, S. W., Seelos, F. P., & Tornabene, L. L. (2009). Diverse aqueous environments on ancient Mars revealed in the southern highlands. *Geology*, *37*(11), 1043–1046. <https://doi.org/10.1130/G30331A.1>
- Wyatt, M. B., & McSween, H. Y. (2002). Spectral evidence for weathered basalt as an alternative to andesite in the northern lowlands of Mars. *Nature*, *417*(6886), 263–266. <https://doi.org/10.1038/417263a>